Journal of Catalysis 268 (2009) 115–121

Contents lists available at ScienceDirect

Journal of Catalysis

journal homepage: www.elsevier.com/locate/jcat

# CO/NO and CO/NO/$O_2$ reactions over a Au–Pd single crystal catalyst

Feng Gao, Yilin Wang, D. Wayne Goodman *

*Department of Chemistry, Texas A&M University, P.O. Box 30012, College Station, TX 77842-3012, United States*

ARTICLE INFO

*Article history:*
Received 21 July 2009
Revised 24 August 2009
Accepted 5 September 2009
Available online 2 October 2009

*Keywords:*
AuPd(1 0 0)
Alloy
Model catalyst
CO oxidation
NO reduction
Surface segregation
Polarization modulation
Infrared reflection absorption spectroscopy
Reaction kinetics

ABSTRACT

NO reduction by CO was investigated over a AuPd(1 0 0) model catalyst at near atmospheric pressures. The alloy catalyst exhibits higher $CO_2$ formation rates below ~550 K than does pure Pd, although the binding energy of NO on the alloy surface is substantially less, i.e., its dissociation tendency is much less, compared with pure Pd. This behavior is rationalized by the fact that the low CO/NO-binding energies with the alloy surface provide a substantial population of empty ensembles for NO dissociation at relatively low temperatures. Moreover, AuPd(1 0 0) catalyzes the CO + NO reaction with much higher $N_2$ selectivity than does pure Pd. Reaction kinetics data reveal that contiguous Pd sites are essential for NO dissociation. The reaction orders in CO and NO pressures, vastly different from Pd and Rh, are also a consequence of the low-binding energies of CO and NO on the alloy surface. It is also found that low-pressure NO promotes the CO + $O_2$ reaction via gas-phase $NO_2$ formation; the latter dissociates to form $O_{(ads)}$ more efficiently than does $O_2$ below ~600 K. However, when the NO pressure exceeds a critical value, gas-phase $NO_2$ causes surface oxidation and thus inhibits $CO_2$ formation. The current study suggests that AuPd alloys should be superior catalysts compared to traditional catalysts with respect to the "cold start" problem in catalytic automobile pollutant removal.



## 1. Introduction

Since the 1970s, three-way catalysts (TWCs) have been used in the automobile industry to simultaneously (i) oxidize CO to $CO_2$, (ii) reduce $NO_x$ to $N_2$, and (iii) combust unburnt hydrocarbons [1–6]. The first generation TWCs were Pt/Rh (90/10) catalysts. Although Rh exhibits superior properties compared with Pt and Pd with respect to $NO_x$ removal and low-temperature CO oxidation, it is scarce and thus expensive [3,7]. In the mid-1990s a new generation of Pd-only TWCs was developed consisting of Pd particles deposited on a high surface area oxide (typically γ-alumina) support with varying amounts of stabilizers and promoters such as $CeO_2$, $SiO_2$, $La_2O_3$, and BaO [8]. While the total cost of Pd-only TWCs is near that of Pt/Rh TWCs, it is preferred since Rh is not required. Moreover, Pd-only TWCs exhibit excellent durability [6]. However Pd-only TWCs have their disadvantages, a prominent one being the so-called "cold start" problem, i.e., the poor performance of Pd TWCs at low temperatures. Although this problem is not unique for Pd, this problem is amplified in Pd TWCs by the absence of Rh, which offers better $NO_x$ removal and low-temperature CO oxidation activity compared with Pd and Pt [1–6].

Over the past several decades, an in-depth knowledge of the mechanisms and kinetics of chemical reactions relevant to catalytic pollutant removal has been obtained using the so-called surface science approach, i.e., using model catalysts (single crystals and supported particles/thin films on planar substrates) at pressures from ultrahigh vacuum to practical conditions [9–24]. As such, the inefficiency of Pd catalysts under certain conditions (for example, at low temperatures) is well understood. First, the low reactivity of Pd in catalyzing CO oxidation at relatively low temperatures is due to the well-known CO inhibition phenomenon [16–18,22–24]. That is, the Pd surface is predominantly covered by CO near room temperature such that the surface becomes very inefficient in adsorbing and dissociating $O_2$ for CO oxidation. This arises due to the rather high-binding energy of CO with pure Pd [9]. Clearly, decreasing the binding energy of CO reduces this inhibition factor which, in turn, reduces the light-off temperature of a working catalytic converter. Secondly, Pd-only catalysts are not very effective and selective in $NO_x$ reduction. In terms of selectivity, the ideal nitrogen-containing product during $NO_x$ reduction is $N_2$. As mentioned above, Rh offers higher activity and better selectivity ($N_2$ versus $N_2O$ and/or $NH_3$) compared with Pd [6]. Studies have shown that the less-ideal parallel reaction pathway $2NO + CO \rightarrow N_2O + CO_2$ occurs at very high selectivity on pure Pd [25–27]. This can be rationalized simply by the low dissociation probability and higher binding energy of NO on Pd leading to the coexistence of high surface coverages of $N_{(ads)}$ and $NO_{(ads)}$. This, in turn, leads to higher yields of $N_2O$. Even for Rh, although the overall reactivity is higher, $N_2$ selectivity is not satisfactory below ~800 K [28]. Because of the stricter standards for nitrogen emissions from automobiles, there has been an intense search for materials that are more selective in catalyzing $N_2$ formation. Accordingly, finding a suitable replacement for Rh is highly

* Corresponding author. Fax: +1 979 845 6822.
*E-mail address:* goodman@mail.chem.tamu.edu (D.W. Goodman).

0021-9517/$ - see front matter © 2009 Elsevier Inc. All rights reserved.
doi:10.1016/j.jcat.2009.09.009

desirable both economically and environmentally. However, finding other metals that are more efficient in NO dissociation (the key step in $NO_x$ reduction) without losing reactivity toward CO oxidation and hydrocarbon combustion is a daunting challenge.

Very recent US patents for exhaust catalysts using PdAu alloys (preferentially at Au/Pd ratios of ~0.8) in combination with other precious metals (Pt, PtPd alloy, PtBi alloy, etc.) report substantially reduced CO and hydrocarbon emissions. Unfortunately these catalysts with PdAu alone do not perform very well in that they typically do not exhibit good hydrocarbon combustion activity [29]. In this investigation a AuPd(1 0 0) single crystal has been used as a model catalyst to study CO oxidation and CO + NO reactions at conditions found typically in an automotive converter, i.e., reactions at or near stoichiometry, CO pressures of ~0.01 atm, and temperatures between 300 and 800 K. A study of CO + $O_2$ has been reported in detail elsewhere [30,31]. Briefly, we found high reactivity (orders of magnitude higher than pure Pd) below ~500 K, due primarily to the low-binding energies of CO with the AuPd(1 0 0) surface such that CO inhibition is greatly reduced. In the present study, we report the results of CO + NO and CO + NO + $O_2$ reactions.

## 2. Experimental section

Polarization-modulation infrared reflection absorption spectroscopy (PM-IRAS) and reaction kinetics measurements were the primary methods used in this study. The experimental apparatus has been described in detail previously [22–24]. Briefly, the apparatus consists of two parts: (1) an ultrahigh vacuum (UHV) section equipped with Auger spectroscopy (AES), low energy electron diffraction (LEED), a UTI 100 mass spectrometer (QMS), and (2) a high-pressure reaction cell. The AuPd(1 0 0) bulk alloy single crystal (Matek, bulk Au/Pd ratio 1/1) was cleaned by repeated ion sputtering at room temperature, followed by annealing at 800 K for 20–30 min [32]. The cleanliness of the sample was verified by AES. The annealing allowed an equilibrium concentration of surface Pd and Au to be reached. Previously low energy ion scattering spectroscopy (LEISS) has shown that following this treatment in ultrahigh vacuum, the surface consists of ~10% Pd and ~90% Au [32]. For this PdAu surface CO titration showed that surface Pd atoms are completely isolated by Au [31]. PM-IRAS measurements were carried out using a Bruker Equinox 55 FTIR spectrometer coupled with a polarization modulator to subtract the contribution of the infrared signals from the gas phase. This method allows *in situ* measurements of surface species over a wide range of pressures from UHV to atmospheric. Kinetics measurements were conducted in a batch mode using the high-pressure cell (~1.0 L) attached to and isolable from the UHV chamber. Reaction rates were derived by post-reaction analysis of the gas-phase composition using QMS. CO conversion was kept below 10% to achieve differential reaction rates.

C.P. grade CO (>99.5%, Matheson Tri-Gas) was further purified by passing through a 4A molecule sieve and a liquid nitrogen-cooled trap to remove metal carbonyl impurities. C.P. grade NO (>99%, Matheson Tri-Gas) was purified via multiple cycles of bulb-to-bulb distillation to remove $N_2O$ and $NO_2$ impurities. Ultrahigh purity $O_2$ (Matheson Tri-Gas) and isotopic-labeled gases, e.g., $^{13}CO$, $^{15}NO$, and $^{18}O_2$ (ICON, >99%) were used as received.

## 3. Results and discussion

### 3.1. CO + NO reaction

The CO + NO reaction can be described by two global reaction pathways, one leading to the desired product $N_2$, and a second, to the undesirable product $N_2O$ [25]:

$$CO + NO = CO_2 + 1/2N_2 \quad (1)$$

$$CO + 2NO = CO_2 + N_2O \quad (2)$$

In terms of elementary reaction steps, the reaction can be expressed as [26,28,33]:

$$CO_{(g)} \rightleftarrows CO_{(ads)} \quad (3)$$

$$NO_{(g)} \rightleftarrows NO_{(ads)} \quad (4)$$

$$NO_{(ads)} \rightarrow N_{(ads)} + O_{(ads)} \quad (5)$$

$$NO_{(ads)} + N_{(ads)} \rightarrow N_2 + O_{(ads)} (\delta\text{-}N_2) \quad (6)$$

$$2N_{(ads)} \rightarrow N_2 (\beta\text{-}N_2) \quad (7)$$

$$NO_{(ads)} + N_{(ads)} \rightarrow N_2O \quad (8)$$

$$CO_{(ads)} + O_{(ads)} \rightarrow CO_2 \quad (9)$$

Note that this is not a complete set of reactions that might be involved. For example, studies have shown the formation and decomposition of an isocyanate (NCO) intermediate [34]. During the course of this study, however, no evidence was found for the formation of an isocyanate species (characterized by infrared vibrational frequencies at ~2240 $cm^{-1}$ [34]) on the alloy surface under any of the reaction conditions investigated. Note also that the involvement of step (6) is necessary to explain recent isotope-labeled molecular beam data [35–37] and this notion has been discussed in detail elsewhere [38].

The first goal of this study was the determination of the global pathway, (1) and (2), that dominates on AuPd(1 0 0). This is especially important since this determines whether a QMS can be used to monitor the reaction products. Obviously if unlabeled NO (30 amu) is used, CO and $N_2$ (both 28 amu) and $CO_2$ and $N_2O$ (both 44 amu) cannot be distinguished mass spectrometrically. On the other hand, $CO_2$ and $N_2O$ are easily distinguished using infrared spectroscopy. However, our experimental setup only allows IRAS to be used to monitor either the surface species or the gas-phase composition, but not both simultaneously. Fig. 1 presents typical gas-phase spectra of the $CO_2$ and $N_2O$ stretching vibrational regions under similar reaction conditions for a CO/NO (1/1) mixture at a total pressure of 8 Torr and at the point where the CO conversion has reached ~40% (in order to form enough products for a reliable analysis). The results for reaction at 700 K over Pd(1 0 0) are shown in the bottom curve and for 650 K over AuPd(1 0 0) in the upper curve. It is evident that $N_2O$, which forms on pure Pd [25–27] (marked with the shaded area), is not detected in the gas phase over AuPd(1 0 0). The lack of $N_2O$ formation over the alloy surface was further probed using $^{15}NO$ as the reactant. Note that by using this isotope, all reactants and products are readily distinguished via QMS. Indeed, it is apparent that $^{15}N_2$ (30 amu) is dominant, while $^{15}N_2O$ (46 amu) is below ~5% of the nitrogen-containing products, using a CO/NO (1/1) mixture and a variety of reaction temperatures and CO conversions (data not shown). The above results demonstrate that the global reaction pathway (1) dominates on a AuPd(1 0 0) catalyst, confirming the efficacy of using unlabeled NO (30 amu) as the reactant and using QMS to monitor the formation of $CO_2$ (44 amu). This allows PM-IRAS to be used to monitor the surface species.

The data for the $CO_2$ formation rate (in turnover frequency (TOF), i.e., $CO_2$ molecule per surface site per second) versus reaction temperature are shown in Fig. 2a as an Arrhenius plot, using 4 Torr CO and 4 Torr NO as the reactants. Note that the dominance of global path (1) indicates that the reaction kinetics of $N_2$ formation mimics that of $CO_2$. Two key points need to be addressed with respect to Fig. 2: (1) the $CO_2$ formation rate below ~500 K is rather high. This is in sharp contrast to the data for pure Pd which has a much lower reactivity at similar low temperatures [25–27]; and (2) two kinetic regimes are apparent: a lower activation energy

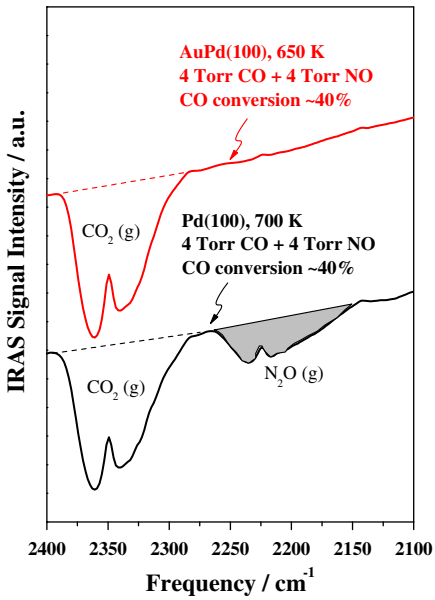


**Fig. 1.** Gas-phase infrared spectra in the 2400–2100 $cm^{-1}$ region acquired in the middle of the CO + NO reaction. The reaction was carried out using 4 Torr CO and 4 Torr NO as the reactants and the spectra were acquired at CO conversion of ~40%. Upper curve: AuPd(1 0 0) sample, reaction temperature 650 K; bottom curve: Pd(1 0 0) sample, reaction temperature 700 K. Note that $N_2O$ (the shaded area) forms using the Pd(1 0 0) model catalyst but not with AuPd(1 0 0).

regime below ~500 K and a higher activation energy regime above ~500 K.

Fig. 2b presents the corresponding *in situ* PM-IRAS spectra as a function of temperature. Based on the recent detailed CO PM-IRAS measurements on the same surface [30,31], as well as previous studies addressing coadsorption of CO and NO on Pd surfaces [25,39], assignments of the CO and NO bands can be precisely made as follows: (1) the CO band at 2120 $cm^{-1}$ (which becomes undetectable above 350 K) is assigned to CO adsorbed on Au sites; (2) the bands at 2040–2080 and 1900–2000 $cm^{-1}$ are assigned to CO adsorption on isolated and contiguous Pd sites, respectively; and (3) the bands at 1710–1780 and 1600–1670 $cm^{-1}$ are assigned to NO adsorption on isolated and contiguous Pd sites, respectively. Adsorption of NO on Au sites is not detected. Note that adsorption on isolated Pd sites can only be on top; for bridge adsorption at least two neighboring Pd atoms (contiguous) are necessary.

Two key points can be derived from the PM-IRAS spectra. First, the CO-binding energy to various surface sites follows the trend, isolated Pd sites > contiguous Pd sites > Au sites. (Note that the same trend was found for CO alone and CO + $O_2$ mixtures [30,31] on the same surface.) Secondly, the CO and NO compete for the same surface sites. Previous studies have shown that on pure Pd surfaces, NO and CO have comparable sampling cross-sections [25]. By analogy we assume similar cross-sections for NO and CO adsorbed on Pd sites within the alloy. It is then clear from Fig. 2b that the ever present smaller NO signal intensities compared with CO leads to the conclusion that for the CO/NO (1/1) mixture, although the $\Theta_{NO}/\Theta_{CO}$ ratio increases with increasing temperature, the NO surface coverage ($\Theta_{NO}$) is always smaller than $\Theta_{CO}$. This then implies that the binding energy of NO is smaller than CO on the AuPd(1 0 0) surface. Recently we have found that the binding energy of CO to AuPd(1 0 0) is rather weak (⩽84 kJ/mol) [31]. Note that on pure Pd, the binding energy of NO is similar (slightly higher) to that of CO such that $\Theta_{NO}$ is generally comparable or slightly higher than $\Theta_{CO}$ under reaction conditions when the CO/NO ratio in the gas phase is comparable [25,39]. The binding energy of CO with Pd surfaces has been investigated in detail previously. For example, the isosteric heat of adsorption of CO on Pd(1 0 0) is ~153 kJ/mol at low coverages [9]. The marked difference between the binding of CO and NO to pure Pd compared with a AuPd alloy is not fully understood but likely relates to an electronic (ligand) effect. The increase in the $\Theta_{NO}/\Theta_{CO}$ ratio with increasing temperature, on the other hand, can be rationalized by an increase in repulsion between NO and neighboring molecules compared with the corresponding CO repulsions at lower temperatures (where the total coverage is higher) such that $NO_{(ads)}$ is more easily replaced by $CO_{(ads)}$. This can simply be caused by the

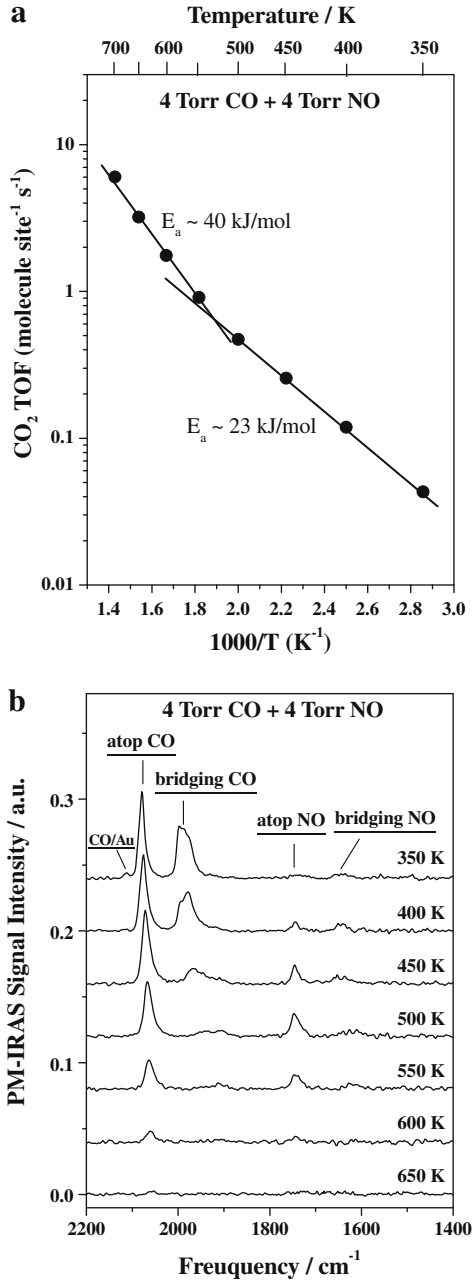


**Fig. 2.** (a) $CO_2$ formation rate (in TOF) as a function of reaction temperature in an Arrhenius plot. The reaction was carried out using 4 Torr CO and 4 Torr NO as the reactants. Reaction rate was calculated through post-reaction QMS analysis of the gas phase. The CO conversion was maintained below ~5% to acquire differential reaction rate. Note two reaction regimes below and above ~500 K. (b) The corresponding *in situ* PM-IRAS spectra. The spectra were typically acquired at 1000 scans at a resolution of 4 $cm^{-1}$. Reaction temperatures and CO and NO band assignments are marked adjacent to the spectra.

larger van de Walls radius of NO compared with CO [25]. The combination of reaction kinetics and *in situ* PM-IRAS leads to a seemingly paradoxical situation, i.e., the weak interaction between NO and the alloy surface indicates that NO is more difficult to dissociate compared to pure Pd, while the kinetic data show that the low-temperature reactivity of AuPd(1 0 0) is higher than pure Pd (note that the elementary reaction step (5) is a prerequisite for all other reaction steps). This behavior can be understood, however, from simple kinetic arguments. On pure Pd and at relatively low temperatures, the surface is saturated with $CO_{(ads)}$ and $NO_{(ads)}$ such that NO dissociation is limited by the availability of empty surface ensembles of sufficient size. Surface reaction could be further limited by the accumulation of $N_{(ads)}$. On AuPd(1 0 0), on the other hand, the low-binding energy of CO/NO with the surface enables properly sized empty ensembles to form more easily. Post-reaction Auger spectroscopic analysis does not indicate a measurable quantity of $N_{(ads)}$ on the surface under any reaction conditions, further corroborating the argument that the alloy surface is much less inhibited by adsorbates.

Overall, the reaction kinetics of the CO + NO reaction by AuPd(1 0 0) versus pure Pd are comparable to the reaction kinetics found for the $CO + O_2$ reaction catalyzed by AuPd(1 0 0) versus pure Pd, i.e., the reaction rate is higher on AuPd(1 0 0) at lower temperatures (<∼550 K) while higher on pure Pd at higher temperatures [31]. Finally, the two different reaction regimes shown in Fig. 2a may reflect the relative significance of the primary reaction steps (6) and (7) at different temperatures. (The reaction kinetics of $N_2$ mimics that of $CO_2$ shown in the figure, although the product $N_2$ cannot be monitored mass spectrometrically.) A previous study on Rh(1 1 1) [13] suggests that reaction step (6), the δ-$N_2$ pathway, dominates at low temperatures (<∼550 K) while reaction step (7), the β-$N_2$ path, becomes the controlling pathway at higher temperatures due to its higher activation energy and the much lower surface coverage of $NO_{(ads)}$. This behavior appears to be rather general based on the data shown in Fig. 2a.

PM-IRAS spectra shown in Fig. 2b provide insights as to why the formation of $N_2O$, which frequently occurs at high selectivities over Pd and Rh model catalysts below ∼700 K [25–28], is far less favored on AuPd(1 0 0). $N_2O$ formation requires coadsorption of $NO_{(ads)}$ and $N_{(ads)}$, as shown in elementary step (8). $\Theta_{NO}$ is generally high on pure Pd under reaction conditions due to its high-binding energy and low dissociation probability. On pure Rh $\Theta_N$ is generally high, due to the much higher NO dissociation probability. In any case, high coverages of $NO_{(ads)}$ and $N_{(ads)}$ are easily realized at relatively low temperatures on pure Pd and Rh (<∼800 K). However, this is not the case on AuPd(1 0 0). As shown in Fig. 2b, at relatively low temperatures adsorption of CO dominates NO while at high temperatures both molecules have exceedingly low coverages due to their weak binding energies.

We have shown recently that the surface composition of AuPd(1 0 0) can be tuned by varying the reactant pressure during the $CO + O_2$ reaction [30,31]. This is caused by the fact that higher CO pressures induce greater Pd segregation to the surface. In turn, higher Pd coverages were found to facilitate CO oxidation. In this study, similar experiments were performed and the data are shown in Fig. 3. The $CO_2$ formation rates versus reactant pressure in Fig. 3a (CO/NO (1/1) mixtures, total pressure 1–64 Torr), show that the reaction rate increases with increasing reactant pressure, behavior seen for the $CO + O_2$ reaction [30]. The surface composition can be assessed qualitatively by *in situ* PM-IRAS. However, as shown in the right panel of Fig. 3b, at 600 K (the reaction temperature), the surface CO and NO signal intensities become very small, indicating low CO and NO coverages. By cooling the sample to 500 K (middle panel), then further to 350 K (left panel), an increase in signal intensity is apparent and provides insight into the variation of surface composition with gas pressure. It is noteworthy that that the surface composition at 600 K is not necessarily the same as that at 500 and 350 K since Au tends to diffuse to the surface with an increase in temperature, at least in a ultrahigh vacuum environment [32]. However, for simplicity it is assumed that the surface composition does not vary substantially with temperature when exposed to *elevated pressures*. At 350 K all surface Pd sites are fully covered with CO and NO molecules such that the integrated CO and NO signals provide a rather convenient and semi-quantitative assessment of the surface composition [31]. Furthermore, the extent of Pd segregation can be estimated by the variation of atop CO peak area (at ∼2070 $cm^{-1}$, corresponding to the number of isolated Pd sites) and bridging CO peak area (at ∼1990 $cm^{-1}$, corresponding to the number of contiguous Pd sites). As shown in the left panel of Fig. 3b, the extent of Pd segregation increases rapidly with increasing reactant pressures ⩽4 Torr. This is evidenced by the rapid increase in the bridging CO peak area and the concurrent decrease in the atop CO peak area with increasing reactant pressure. At reactant pressures of 8 Torr and higher, it is seen that further Pd segregation essentially stops.

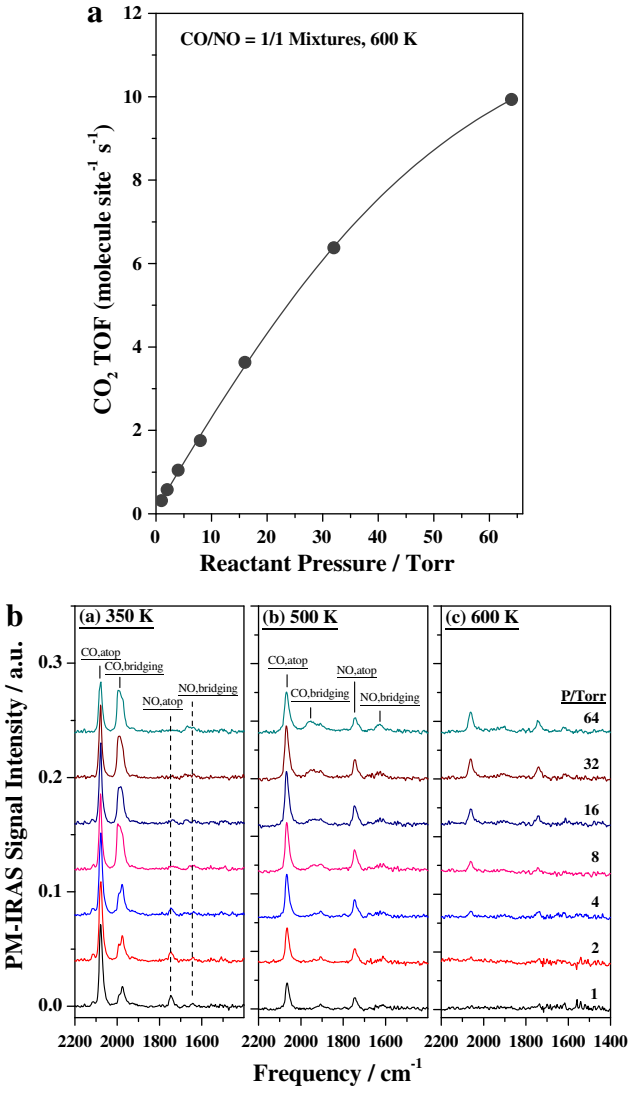


**Fig. 3.** (a) The $CO_2$ formation rate (in TOF) as a function of reactant pressure at a reaction temperature of 600 K. CO/NO (1/1) mixtures were used as reactants with total pressure varying from 1 to 64 Torr. (b) The corresponding *in situ* PM-IRAS spectra acquired as 350 K (left panel), 500 K (middle panel), and 600 K (right panel). The spectra were typically acquired at 1000 scans at a resolution of 4 $cm^{-1}$. Reactant pressures are marked adjacent to the corresponding spectra.

The combination of Fig. 3a and b reveals that the $CO_2$ formation rate approaches zero when the number of surface contiguous Pd sites approaches zero, indicating that these are the sites that are active in NO dissociation. We have shown recently that $O_2$ dissociation occurs exclusively on contiguous Pd sites [30]. However, at reactant pressures of 8 Torr and higher, the number of contiguous Pd sites is essentially constant (left panel, Fig. 3b) while the $CO_2$ formation rate continues to increase with pressure (Fig. 3a). This argues for the involvement of CO adsorbed on Au and isolated Pd sites, especially the former, in the reaction. Fig. 3b also reveals more detailed information regarding the competition of CO and NO on the alloy surface. In particular it is seen that $\Theta_{NO}/\Theta_{CO}$ increases with increasing sample temperature and decreasing gas pressure, i.e., with decreasing total coverage, consistent with a stronger repulsion of NO with neighboring molecules compared with CO as discussed above.

Reaction kinetics was further probed by keeping the pressure of one reactant constant while varying the other, with the goal of measuring the reaction orders in CO and NO pressures. This type of measurement has been found to be very useful in elucidating reaction mechanisms. For instance, at relatively low temperatures the CO + $O_2$ reaction over pure Pd shows +1 order dependence in $O_2$ pressure and −1 order dependence in CO pressure, fully consistent with CO inhibition of the reaction [16–18]. The CO + NO reaction is more complex, and attributed to the interplay of numerous elementary steps as described above. For the CO + NO reaction over supported Pd, ∼−1 order dependence in CO pressure and +1/2 order dependence in NO pressure has been found at 550 K [26]. This behavior is consistent with the inhibition of the reaction by CO. Furthermore, this also suggests that the role of NO is complex, i.e., its dissociation promotes the reaction, whereas site blocking by NO (as with CO) inhibits the reaction. On the other hand, the situation is even more complex on both single crystalline [13,14] and supported [13] Rh, where unusual pressure dependencies have been observed such as zero order (or weak) dependences on both CO and NO. This could nevertheless be rationalized by the high coverage of another surface species, namely $N_{(ads)}$, on Rh surfaces, a situation not realized with Pd surfaces. Fig. 4a displays reaction kinetics data where the left panel shows data acquired by maintaining 8 Torr CO and varying the NO pressure from 0.5 to 64 Torr; the right panel data were acquired by maintaining the NO pressure and varying the CO pressure. Both sets of data were acquired at 650 K. The relatively high reaction temperature was chosen in order to form sufficient product $CO_2$ for post-reaction analysis within a reasonable reaction time. At this reaction temperature, however, surface CO and NO species are barely detectable using PM-IRAS. The adsorbate-covered surfaces were monitored using PM-IRAS at 350 K instead (Fig. 4b). Again we assume that the relative surface composition does not vary substantially between 350 and 650 K. Compared with single metal samples, this type of reactant order dependence measurements using an alloy sample is more complex since the surface composition of an alloy is not invariant; preferential segregation of Pd to the surface is enhanced with increasing reactant pressure. For the experimental conditions used here, i.e., CO + NO total pressures higher than 8 Torr, the surface composition does not appear to vary substantially with varying reactants. This conclusion is derived from integration of the CO and NO peak areas shown in Fig. 4b. Indeed, the total adsorbate peak areas remain constant with varying reactant composition indicating a constant surface composition. At relatively low CO and NO pressures, as shown in Fig. 4a, the positive order dependence toward both reactants reveals that neither of the reactants are inhibitors, consistent with the low-binding energies of CO and NO with the alloy surface, and also consistent with the lack of $N_{(ads)}$ accumulation on the surface as verified by post-reaction AES analysis (data not shown). At fixed total pressures but different

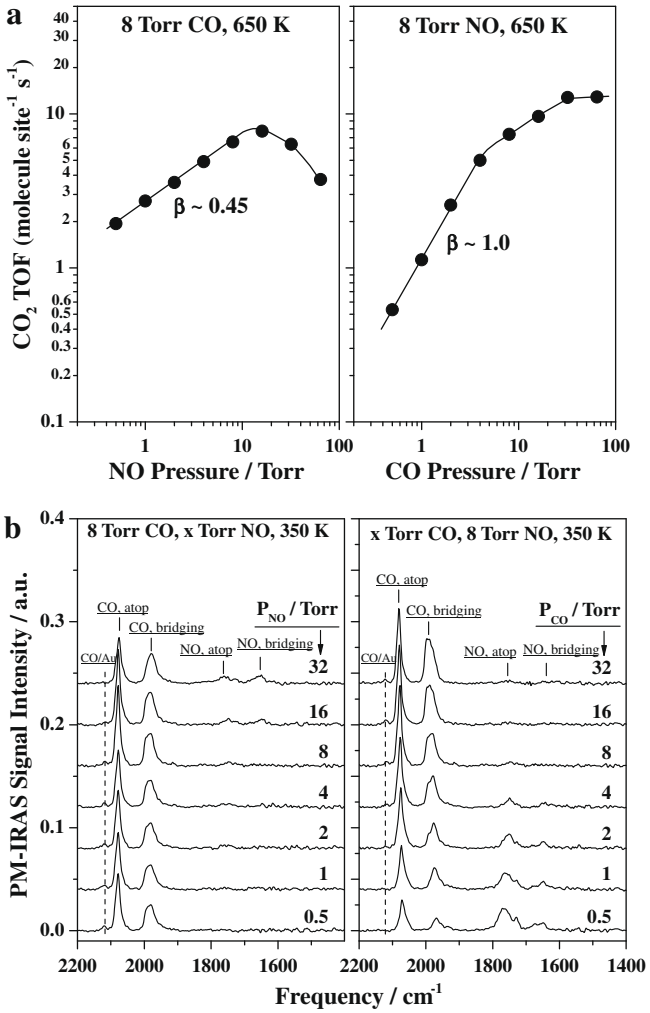


**Fig. 4.** (a) $CO_2$ formation rate (in TOF) at a reaction temperature of 650 K. Left panel: 8 Torr CO and various pressures of NO (0.5–64 Torr) as reactants; right panel: 8 Torr NO and various pressures of CO (0.5–64 Torr) as reactants. (b) The corresponding *in situ* PM-IRAS spectra acquired as 350 K. Left panel: 8 Torr CO and various pressures of NO (0.5–64 Torr) as reactants; right panel: 8 Torr NO and various pressures of CO (0.5–64 Torr) as reactants. The spectra were typically acquired at 1000 scans at a resolution of 4 $cm^{-1}$. NO (CO) pressures and band assignments are marked adjacent to the spectra.

CO/NO ratios (e.g., 8 Torr CO + 1 Torr NO versus 1 Torr CO + 8 Torr NO), CO-rich reactants always display higher $CO_2$ formation rates, suggesting that $N_{(ads)}$ has some adverse effects on $CO_2$ formation.

### 3.2. CO + NO + $O_2$ reaction

Reactions were also carried out in the presence of CO, NO, and $O_2$. At similar reactant pressures and reaction temperatures, we have shown that the CO + $O_2$ reaction proceeds much faster than the CO + NO reaction on AuPd(1 0 0). For example, a $CO_2$ turnover frequency greater than ∼100 molecule $site^{-1}$ $s^{-1}$ was found for the CO + $O_2$ reaction at 500 K [31] while for the CO + NO reaction, the $CO_2$ formation rate is two orders of magnitude smaller (Fig. 2a) at the same temperature and similar CO pressures. As such we focus here on the influence of NO on the CO + $O_2$ reaction. This is done by adding various amounts of NO to fixed CO + $O_2$ mixtures and measuring the reaction kinetics. Previous studies have shown a dramatic influence of NO on CO oxidation reaction catalyzed by Rh and Pd, namely, NO greatly inhibits the CO + $O_2$ reaction over Rh [40] but promotes the reaction over Pd [41] at relatively low

temperatures. NO inhibition over Rh can be understood by $N_{(ads)}$ poisoning. However, NO promotion over Pd is complex and will be discussed in more detail below since the same promotional effect is found for AuPd(1 0 0).

Fig. 5a displays the $CO_2$ formation rate (TOF) at 16 Torr CO, 8 Torr $O_2$, and varying pressures of NO from 0 to 16 Torr; the reaction temperature was 500 K. Adding small amount of NO (⩽4 Torr) clearly promotes $CO_2$ formation, especially at NO pressures of ~2 Torr. Presumably this effect is due to the involvement of $NO_2$ that forms due to the gas-phase reaction between $O_2$ and NO, since direct dissociation of NO at this temperature contributes little to the total $CO_2$ formed (Fig. 2a). $NO_2$ has been known to be a stronger oxidant than $O_2$ and dissociation of this molecule has been used routinely to generate high coverages of oxygen on transition metal surfaces [42,43]. The key reactions involved are as follows:

$$2NO_{(g)} + O_{2(g)} \rightarrow 2NO_{2(g)} \quad (10)$$

$$NO_{2(g)} \rightarrow NO_{2(ads)} \quad (11)$$

$$NO_{2(ads)} \rightarrow NO_{(g)} + O_{(ads)} \quad (12)$$

Such a mechanism also explains the decrease in the $CO_2$ formation rate when excess NO is present in the gas phase. This can simply be caused by oxidation of the alloy sample. It has been demonstrated previously that upon oxidation, Pd oxides have significantly reduced reactivity toward CO oxidation [23]. In order to confirm its role, the quantity of $NO_2$ in the gas phase was first examined using QMS. As shown in Fig. 5b, two linear regimes are found: for NO pressures ⩽4 Torr, a $NO_2$/NO ratio of ~0.01 was observed; for higher NO pres-

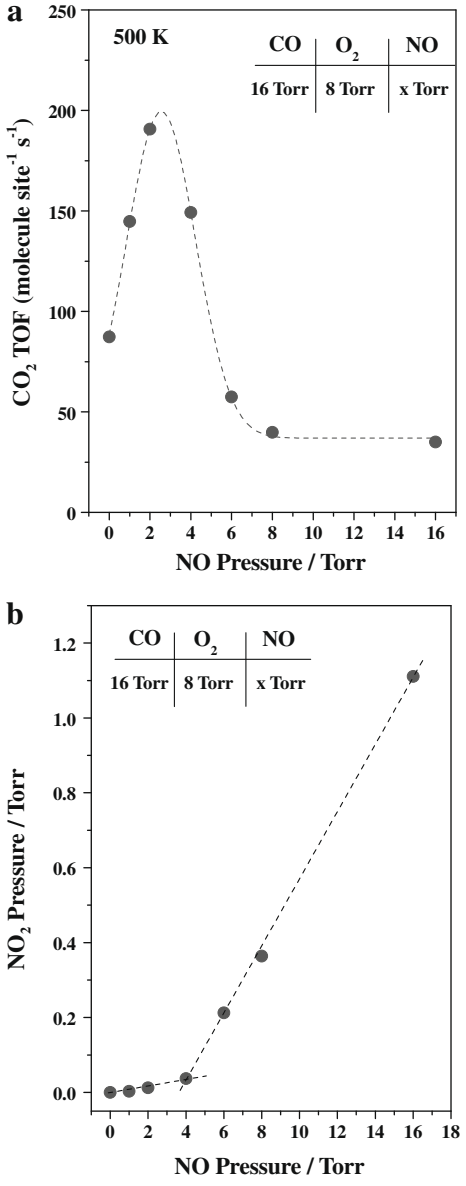


**Fig. 5.** (a) $CO_2$ formation rate (in TOF) at a reaction temperature of 500 K. The reactants were 16 Torr CO, 8 Torr $O_2$, and various pressures of NO from 1 to 16 Torr. Note that NO promotes $CO_2$ formation at pressures ⩽4 Torr while inhibits $CO_2$ formation at higher pressures. (b) $NO_2$ formed in the gas phase after mixing NO with the CO + $O_2$ mixtures, determined using QMS. Note that at NO pressures ⩽4 Torr, gas-phase $NO_2$/NO ratio is ~0.01 while at higher NO pressures $NO_2$/NO ratio becomes ~0.07.

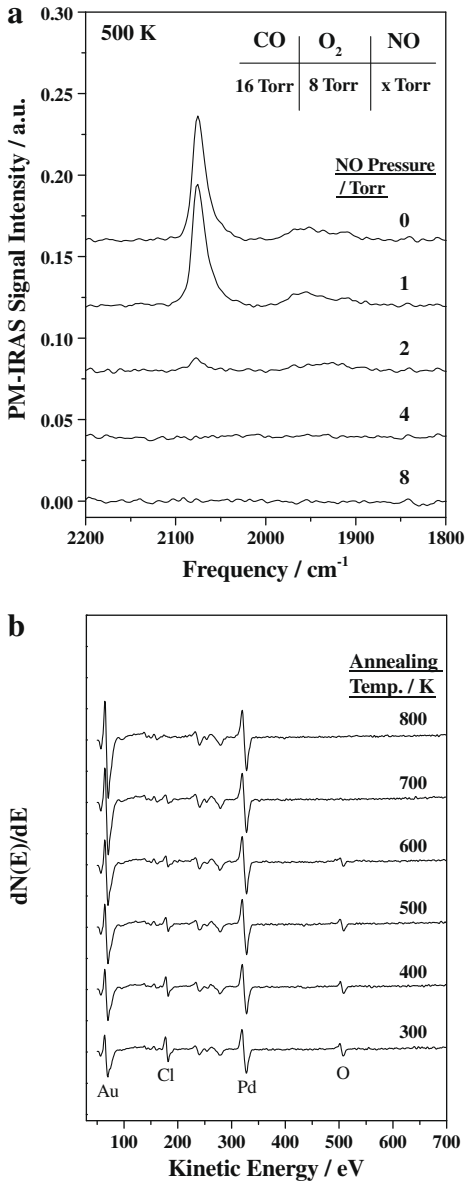


**Fig. 6.** (a) PM-IRAS spectra acquired at a reaction temperature of 500 K. The reactants were 16 Torr CO, 8 Torr $O_2$, and various pressures of NO where NO pressures are marked adjacent to the corresponding spectra. Note that surface CO signal intensity attenuates greatly at a NO pressure of 2 Torr and disappears completely at higher NO pressures. (b) Post-reaction Auger spectrum (bottom curve) of a typical sample exposed to NO pressures higher than 4 Torr during reaction. The spectrum was acquired at a sample temperature of 300 K. The sample oxidation and contamination by Cl are apparent. Temperature-dependent spectra (upper curves, annealing temperatures are marked adjacent to the corresponding spectra) show Pd oxides dissociation below ~700 K and Cl desorption below ~800 K.

sures, the $NO_2$/NO ratio rose to ~0.07. As is clear from Fig. 5a and b, at $NO_2$ pressures lower than ~0.04 Torr, the $CO_2$ formation is promoted while at higher $NO_2$ pressures, the $CO_2$ formation is inhibited.

The surface oxygen coverage increase, caused by reaction (12), can be examined qualitatively using PM-IRAS since the adsorption of oxygen concurrently alters the CO band intensity and frequency. As displayed in Fig. 6a, although adding 1 Torr of NO to the CO + $O_2$ mixture has no apparent effect on the CO signal intensity, upon adding 2 Torr of NO to the gas mixture, the CO signal intensity decreases significantly, consistent with a significant oxygen coverage. Note that this corresponds with the $CO_2$ formation rate data shown in Fig. 5a. It is noteworthy that the surface oxygen remains chemisorbed so long as the gas-phase $NO_2$ pressure remains low. This is apparent from post-reaction AES showing that the surface is essentially free of oxygen (data not shown) upon the addition of $\leqslant$4 Torr of NO to the CO + $O_2$ mixture. This is due to a well-known phenomenon, namely "electron-stimulated-desorption (ESD)" of *chemisorbed* oxygen from a Pd surface [44]. In contrast, oxygen builds up in the subsurface region upon Pd oxidation and can be detected easily with AES. Following the addition of NO to greater than 6 Torr, post-reaction AES data (bottom curve, Fig. 6b) indeed showed clearly a large oxygen feature, consistent with the formation of bulk Pd oxides. Note from Fig. 5a that the $CO_2$ formation rate drops substantially upon the formation of these oxides. This is consistent with our previous studies that bulk Pd oxides are considerably less active than chemisorbed oxygen phases in CO oxidation [23]. Unfortunately, this situation is complicated by the concurrent chlorine contamination of the sample (bottom curve, Fig. 6b). The coverage of Cl is roughly estimated to be ~0.2 ML. The origin of the Cl contamination is not known, however, previous workers have observed similar contamination by Cl after exposure of Pd to large doses of $NO_2$ [45]. It is also apparent from Fig. 6b that dissociation of the Pd oxides occurs below ~700 K while the Cl contaminant desorbs below ~800 K.

Finally, the involvement of reactions (10)–(12) in $CO_2$ formation was probed using $^{18}O_2$ as the reactant. Using labeled oxygen, the dissociation of $N^{16}O^{18}O$ yields equal molar amounts of $^{16}O_{(ads)}$ and $^{18}O_{(ads)}$ on the surface. These, in turn, react with $CO_{(ads)}$ to form $C^{16}O_2$ (44 amu) and $C^{16}O^{18}O$ (46 amu), products easily identified mass spectrometrically. Indeed, using a mixture of $P_{CO}/P_{O_2}/P_{NO} = 8/4/1$, reactions (10)–(12) are shown to play a dominant role in the production of $CO_2$ below ~600 K. Only at higher temperatures does the direct CO + $O_2$ reaction becomes dominant (data not shown). Under realistic operating conditions in TWCs, the NO pressure (ppm level) is substantially lower than the CO and $O_2$ pressures [6], therefore NO under these typical operating conditions should serve solely as a promoter of the CO + $O_2$ reaction.

## 4. Conclusions

In this study the CO + NO and CO + NO + $O_2$ reactions over a bulk alloy model catalyst AuPd(1 0 0) have been investigated using surface spectroscopic and reaction kinetics. The key points found are as follows: (1) alloying with Au greatly reduces the binding energies of CO and NO with Pd. This results in reduced adsorbate inhibition and a corresponding enhanced reactivity at relatively low temperatures. Furthermore, alloying also profoundly affects the product distribution such that $N_2$ is substantially more favored over $N_2O$, compared with pure Pd and Rh. This can be understood by the low $NO_{(ads)}$ and $N_{(ads)}$ coverages evident using *in situ* PM-IRAS and post-reaction AES measurements; (2) the alloy surface composition, i.e., Pd/Au ratio and atomic distribution, varies with the composition and pressure of the reactants. Such changes, sometimes very subtle, can be monitored with PM-IRAS illustrating the usefulness of this technique in providing invaluable in situ data in investigating structure–reactivity relationships.

From a more practical point of view, the current study together with our previous studies on the CO + $O_2$ reaction [30,31] demonstrates an unusual high activity of PdAu at relatively low temperatures (e.g., <500 K) suggesting that the addition of PdAu to traditional TWCs could in principle resolve the so-called "cold start" problem. Furthermore, PdAu alloys may be advantageous compared with pure Pd in high-temperature operation since the alloy is more difficult to oxidize due to electron transfer from Pd to Au [46].

## Acknowledgments

We gratefully acknowledge the support for this work by the Department of Energy, Office of Basic Energy Sciences, Division of Chemical Sciences, Geosciences, and Biosciences (DE-FG02-95ER-14511), and the Robert A. Welch Foundation.

## References

[1] H. Bosch, Catal. Today 2 (1988) 369.
[2] K.C. Taylor, Catal. Rev.-Sci. Eng. 35 (1993) 457.
[3] M. Shelef, G.W. Graham, Catal. Rev.-Sci. Eng. 36 (1994) 433.
[4] R.J. Farrauto, R.M. Heck, Catal. Today 51 (1999) 351.
[5] M. Shelef, R.W. McCabe, Catal. Today 62 (2000) 35.
[6] J. Kašpar, P. Fornasiero, N. Hickey, Catal. Today 77 (2003) 419.
[7] V.I. Pârvulescu, P. Grange, B. Delmon, Catal. Today 46 (1998) 233.
[8] A.H. Tullo, Chem. Eng. News 80 (34) (2002) 17.
[9] T. Engel, G. Ertl, Adv. Catal. 28 (1979) 1.
[10] D.W. Goodman, Chem. Rev. 95 (1995) 523.
[11] S.B. Schwartz, D. Schmidt, G.B. Fisher, J. Phys. Chem. 90 (1986) 6194.
[12] D.W. Goodman, C.H.F. Peden, J. Phys. Chem. 90 (1986) 4839.
[13] S.H. Oh, G.B. Fisher, J.E. Carpenter, D.W. Goodman, J. Catal. 100 (1986) 360.
[14] C.H.F. Peden, D.W. Goodman, D.S. Blair, P.J. Berlowitz, G.B. Fisher, S.H. Oh, J. Phys. Chem. 92 (1988) 1563.
[15] P.J. Berlowitz, C.H.F. Peden, D.W. Goodman, J. Phys. Chem. 92 (1988) 5213.
[16] X. Xu, D.W. Goodman, J. Phys. Chem. 97 (1993) 7711.
[17] J. Szanyi, D.W. Goodman, J. Phys. Chem. B 98 (1994) 2972.
[18] J. Szanyi, D.W. Goodman, J. Phys. Chem. B 98 (1994) 2978.
[19] R.H. Nibbelke, M.A.J. Campman, J.H.B.J. Hoebink, G.B. Marin, J. Catal. 171 (1997) 358.
[20] B.C. Sales, J.E. Turner, M.B. Maple, Surf. Sci. 114 (1982) 381.
[21] J.E. Turner, M.B. Maple, Surf. Sci. 147 (1984) 647.
[22] F. Gao, S.M. McClure, Y. Cai, K.K. Gath, Y. Wang, M.S. Chen, Q.L. Guo, D.W. Goodman, Surf. Sci. 603 (2009) 65.
[23] F. Gao, Y. Wang, Y. Cai, D.W. Goodman, J. Phys. Chem. C 113 (2009) 174.
[24] F. Gao, Y. Cai, K.K. Gath, Y. Wang, M.S. Chen, Q.L. Guo, D.W. Goodman, J. Phys. Chem. C 113 (2009) 182.
[25] S.M. Vesecky, P. Chen, X. Xu, D.W. Goodman, J. Vac. Sci. Technol. A 13 (1995) 1539.
[26] D.R. Rainer, M. Koranne, S.M. Vesecky, D.W. Goodman, J. Phys. Chem. B 101 (1997) 10769.
[27] D.R. Rainer, S.M. Vesecky, M. Koranne, W.S. Oh, D.W. Goodman, J. Catal. 167 (1997) 234.
[28] H. Permana, K.Y. Simon Ng, C.H.F. Peden, S.J. Schmieg, D.K. Lambert, D.N. Belton, J. Catal. 164 (1996) 194.
[29] K.L. Fujdala, T.J. Truex, US Patent 20,080,125,308, 20,080,125,313, 20,080,124,514.
[30] F. Gao, Y. Wang, D.W. Goodman, J. Am. Chem. Soc. 131 (2009) 5734.
[31] F. Gao, Y. Wang, D.W. Goodman, J. Phys. Chem. C 113 (2009) 14993.
[32] P. Han, S. Axnanda, I. Lyubinetsky, D.W. Goodman, J. Am. Chem. Soc. 129 (2007) 14355.
[33] K.Y.S. Ng, D.N. Belton, S.J. Schmieg, G.B. Fisher, J. Catal. 146 (1994) 394.
[34] E. Ozensoy, C. Hess, D.W. Goodman, J. Am. Chem. Soc. 124 (2002) 8524.
[35] F. Zaera, C.S. Gopinath, Chem. Phys. Lett. 332 (2000) 209.
[36] F. Zaera, S. Wehner, C.S. Gopinath, J.L. Sales, V. Gargiulo, G. Zgrablich, J. Phys. Chem. B 105 (2001) 7771.
[37] F. Zaera, C.S. Gopinath, J. Chem. Phys. 116 (2002) 1128.
[38] L.A. Avalos, V. Bustos, R. Unac, F. Zaera, G. Zgrablich, J. Mol. Catal. A: Chem. 228 (2005) 89.
[39] X. Xu, P. Chen, D.W. Goodman, J. Phys. Chem. 98 (1994) 9242.
[40] S.H. Oh, J.E. Carpenter, J. Catal. 101 (1986) 114.
[41] G.W. Graham, A.D. Logan, M. Shelef, J. Phys. Chem. 97 (1993) 5445.
[42] G. Zheng, E.I. Altman, Surf. Sci. 462 (2000) 151.
[43] A. Böttcher, H. Niehus, S. Schwegmann, H. Over, G. Ertl, J. Phys. Chem. B 101 (1997) 11185.
[44] T.E. Madey, J.T. Yates, J. Vac. Sci. Technol. 8 (1971) 525.
[45] G.W. Graham, A.D. Logan, M. Shelef, J. Phys. Chem. 98 (1994) 1746.
[46] A. Kotsifa, T.I. Halkides, D.I. Kondarides, X.E. Verykios, Catal. Lett. 79 (2002) 113.